Check for updates

JGR Oceans

RESEARCH ARTICLE
10.1029/2021JC018309

Wind-Driven Freshwater Export at Cape Farewell

E. Duyck[1], R. Gelderloos[2], and M. F. de Jong[1]

[1]Department of Ocean Systems, NIOZ, Royal Netherlands Institute for Sea Research, Texel, The Netherlands, [2]Department of Earth and Planetary Sciences, The Johns Hopkins University, Baltimore, MD, USA

Key Points:

- Westerly winds at Cape Farewell drive enhanced transport of surface waters across the shelfbreak and extend the salinity front offshore
- Westerly tip jets lead to the strongest export and can impact the water column up to 100 m deep, especially over Eirik Ridge
- Sea ice at Cape Farewell veers eastwards in response to westerly winds, but export at the shelfbreak is minimal compared to liquid export

Correspondence to:
E. Duyck,
elodie.duyck@nioz.nl

Citation:
Duyck, E., Gelderloos, R., & de Jong, M. F. (2022). Wind-driven freshwater export at Cape Farewell. *Journal of Geophysical Research: Oceans*, *127*, e2021JC018309. https://doi.org/10.1029/2021JC018309

Received 2 DEC 2021
Accepted 17 APR 2022

Abstract Increased freshwater input to the Subpolar North Atlantic from Greenland ice melt and the Arctic could strengthen stratification in deep convection regions and impact the overturning circulation. However, freshwater pathways from the east Greenland shelf to deep convection regions are not fully understood. We investigate the role of strong wind events at Cape Farewell in driving surface freshwaters from the East Greenland Current to the Irminger Sea. Using a high-resolution model and an atmospheric reanalysis, we identify strong wind events and investigate their impact on freshwater export. Westerly tip jets are associated with the strongest and deepest freshwater export across the shelfbreak, with a mean of 37.5 mSv of freshwater in the first 100 m (with reference salinity 34.9). These wind events tilt isohalines and extend the front offshore, especially over Eirik Ridge. Moderate westerly events are associated with weaker export across the shelfbreak (mean of 15.9 mSv) but overall contribute to more freshwater export throughout the year, including in summer, when the shelf is particularly fresh. Particle tracking shows that half of the surface waters crossing the shelfbreak during tip jet events are exported away from the shelf, either entering the Irminger Gyre, or being driven over Eirik Ridge. During strong westerly wind events, sea ice detaches from the coast and veers toward the Irminger Sea, but the contribution of sea ice to freshwater export at the shelfbreak is minimal compared to liquid freshwater export due to limited sea ice cover at Cape Farewell.

Plain Language Summary The Atlantic circulation brings warm surface waters from the tropics to the poles, where deep, cold waters are formed and brought back to the tropics, thus redistributing heat across the Atlantic. Climate change leads to increased melt of the Greenland ice sheet and a freshening of the Arctic Ocean. If this additional freshwater reaches regions where deep waters are formed, it could weaken this deep water formation and consequently the Atlantic circulation. Since this could lead to large-scale climate impacts, we need to better understand the pathways between freshwater sources and these regions. The present study investigates wind-driven freshwater export from the east Greenland shelf to the Irminger Sea, southeast of Greenland. We find that strong westerly winds are associated with surface waters export offshore, with part of the exported waters entering the Irminger Sea. How much freshwater enters the Irminger Sea and the possible impact on deep water formation are subject to further research.

1. Introduction

The Atlantic Meridional Overturning Circulation (AMOC) is a critical element of the climate system. It redistributes heat and freshwater across the Atlantic and stores carbon in the deep ocean (Buckley & Marshall, 2016). With continued global warming, the overturning circulation is predicted to weaken, possibly leading to large-scale remote impacts (Collins et al., 2019).

One mechanism that could lead to a slow-down of the AMOC is an increase in freshwater input to the Subpolar North Atlantic deep convection regions (Manabe & Stouffer, 1995; Weijer et al., 2019). The freshening of the Arctic, predicted to strengthen in the coming decades (Haine et al., 2015), and the accelerated melt of the Greenland ice sheet (Bamber et al., 2018; Shepherd et al., 2020), can lead to increasing freshwater input to the Greenland shelf. If this additional freshwater reaches the deep convection regions of the Subpolar North Atlantic, it could strengthen stratification in these regions, thereby dampening deep convection and impacting the overturning circulation (Aagaard & Carmack, 1989). This mechanism was observed in the Labrador Sea during the Great Salinity Anomaly of 1969–1972 (Gelderloos et al., 2012), which originated from Fram Strait and led to an extra 10,000 km^3 of freshwater circulating in the North Atlantic (Dickson et al., 1988). However, freshwater pathways from the boundary current on the Greenland shelf to convection regions are still unclear, and model studies disagree on the timescale at which additional freshwater input from Greenland and the Arctic could have a significant impact on the overturning circulation (Bakker et al., 2016; Böning et al., 2016; Dukhovskoy et al., 2016).

© 2022. The Authors.
This is an open access article under the terms of the Creative Commons Attribution License, which permits use, distribution and reproduction in any medium, provided the original work is properly cited.

In particular, there is little understanding of possible freshwater pathways from the southeastern Greenland shelf into the Irminger Sea. Recent results found the Irminger Sea to be of greater importance than the Labrador Sea in driving variability of the overturning circulation (Li et al., 2021; Lozier et al., 2019; Petit et al., 2020), but most studies to date have focused on freshwater export in the Labrador Sea and its impact in this region (e.g., Pennelly et al., 2019; Yang et al., 2016).

On the east Greenland shelf, freshwater is contained within the East Greenland Current (EGC), which flows along the east Greenland coast from Fram Strait to Cape Farewell. The main branch is located at the shelfbreak and separates the cold and fresh waters flowing south from Fram Strait from the warmer and saltier Irminger Current waters (Figure 1a). An even fresher coastal branch, referred to as the East Greenland Coastal Current, is located over the shelf, carrying Greenland meltwater and Arctic waters equatorwards (Bacon et al., 2014; Foukal et al., 2020; Le Bras et al., 2018). At Cape Farewell, the EGC rounds the cape to become the West Greenland Current. Freshwater export from the boundary current to interior seas is well documented on the western side of Greenland, where both eddies (Hátún et al., 2007; Lilly et al., 2003) and winds (Schulze Chretien & Frajka-Williams, 2018) bring fresh surface waters to the Labrador Sea. On the eastern side of Greenland, surface freshwater is exported from the Greenland shelf north of Denmark Strait to the Nordic Seas, mainly via the Jan Mayen and East Icelandic Current (Dodd et al., 2009; Håvik et al., 2017). Freshwater export from the southeast Greenland shelf to the Irminger Sea is expected to be much weaker and is not well documented.

A drifter deployment conducted on the eastern Greenland shelf in August 2019 suggested that wind events at Cape Farewell could lead to short-lived freshwater export toward the Irminger Sea (Duyck & de Jong, 2021). The Cape Farewell region is the windiest location of the world's oceans (Sampe & Xie, 2007). The interaction of synoptic scale cyclones with the high topography of southern Greenland creates strong wind events called tip jets (Moore, 2003; Moore & Renfrew, 2005). Westerly tip jets are meso-scale (200–400 km) events that are usually short in duration (about 1 day), and can reach 30 m s^{-1} at the surface. They result from the deflection and acceleration of westerly flow at the tip of Greenland, as well as acceleration down the slope at Cape Farewell (Doyle & Shapiro, 1999; Moore, 2003; Våge et al., 2009). Westerly tip jets are characterized by a strong westerly flow over the Irminger Sea, that creates heat fluxes of up to 600 W m^{-2} and contributes to deep convection (Pickart et al., 2003; Våge et al., 2008, 2009). Easterly, or reverse, tip jets are strong northeasterly wind events (Moore, 2003, 2012) that can also reach 30 m s^{-1} at the surface and flow along and south of the east Greenland shelf (Outten et al., 2009; Renfrew et al., 2009). Northeasterly events result from barrier flows adjusting to the loss of the barrier at the tip of Greenland (Moore & Renfrew, 2005; Renfrew et al., 2009). In the following, these two types of extreme wind events occurring at Cape Farewell will be referred to as tip jets and strong northeasterlies. The occurrence of these winds is strongly dependent on background synoptic conditions and the position of the cyclone center, to the northeast or south of Cape Farewell, respectively, allowing for the generation of tip jets and strong northeasterly wind events (Bakalian et al., 2007; Moore, 2003). These strong wind events are likely to influence surface waters and sea ice cover at Cape Farewell. Tip jets in particular could drive fresh waters and sea ice off the shelf, into the Irminger Sea. Deep convection takes place within the Irminger Gyre, both in the gyre center situated east of Cape Farewell (de Jong et al., 2012, 2018; Våge et al., 2011) and south of Cape Farewell (de Jong et al., 2012; Piron et al., 2016, 2017). Liquid or solid freshwater export off the shelf in this area could impact the stratification of this deep convection region.

The study presented here investigates wind-driven export events in the Cape Farewell area using results from a high-resolution simulation of the area (Almansi et al., 2017), atmospheric reanalysis data and satellite observations. Section 2 will describe the datasets used, as well as the methods employed to identify extreme wind events and to compute freshwater export. Section 3 presents the wind events identified using the above method. Section 4 investigates the wind-driven liquid freshwater export and Section 5 expands this to sea ice export. Finally, Section 6 discusses the relevance of these results for convection regions.

2. Methods

2.1. Models and Data

Wind-driven freshwater export at Cape Farewell is investigated using results from a high-resolution simulation based on the Massachusetts Institute of Technology General Circulation Model (MITgcm; Marshall et al., 1997). The configuration and forcing are described by Almansi et al. (2017), and updated as by Almansi et al. (2020).

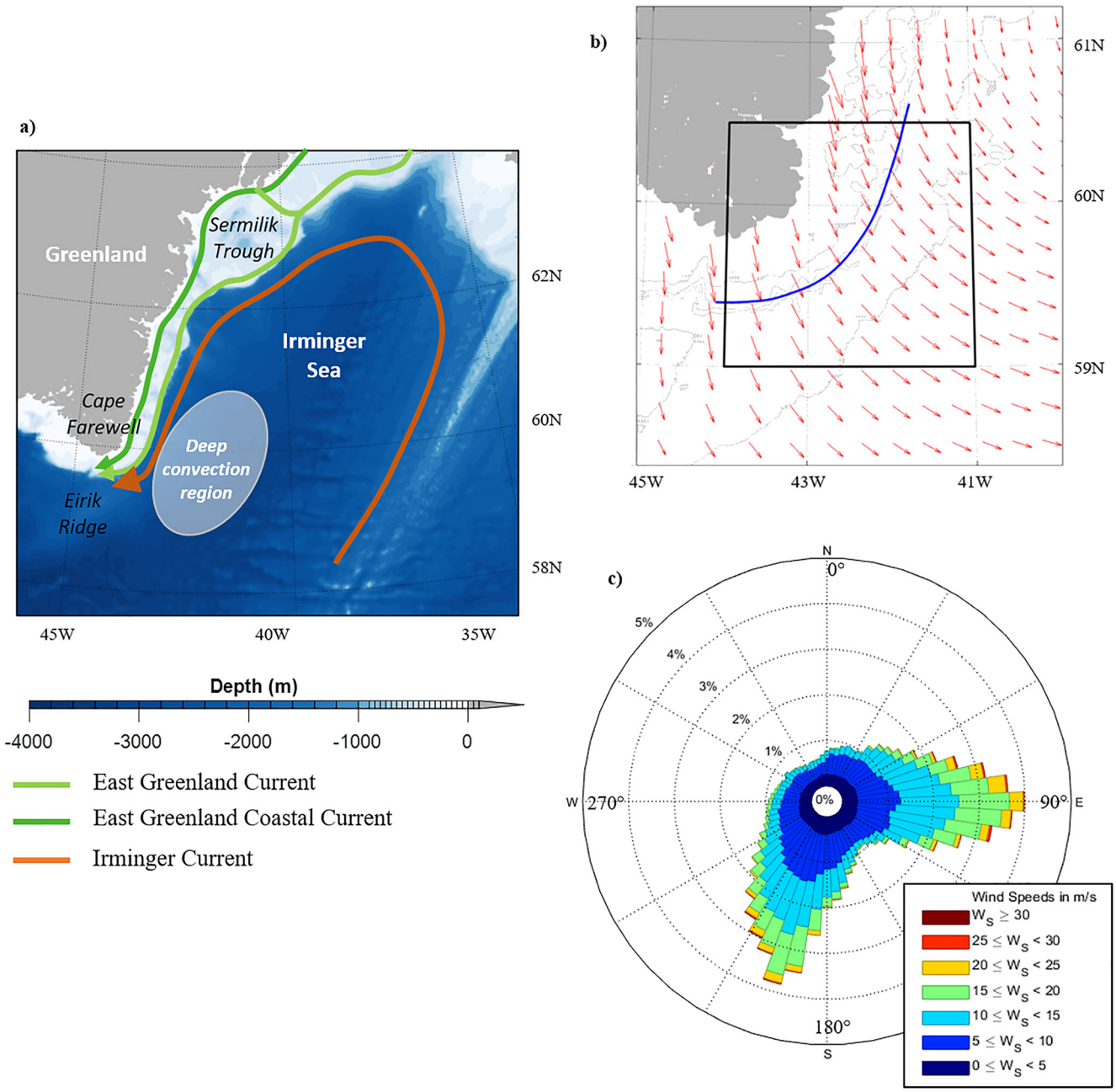

Figure 1. (a) Overview of surface currents and topographic features along the southeast Greenland shelf. (b) Mean winds at Cape Farewell (red arrows), area of interest for wind computations (black), and shelfbreak defined as the smoothed 800 m isobath (blue), bathymetry in gray: 200, 500, 800, 1,000, and 2,000 m. (c) Wind rose for the area of interest.

The horizontal domain covers 47°W–1°E and 57–76°N, discretized with an unevenly spaced grid with resolution of 2 km at the center and 4 km in peripheral areas (including our study area at Cape Farewell). The vertical domain consists of 216 levels, with resolution linearly increasing from 1 to 15 m in the first 120 m and equal to 15 m beyond 120 m depth. The model is forced with the 15-km resolution Arctic System Reanalysis version 2 (ASR-2; Bromwich et al., 2018). Due to its high resolution, the model was run for only 1 yr, from September 2007 to August 2008. The output is available at 6-hr resolution and retrieved from SciServer (Medvedev et al., 2016). We retrieved the 10-m wind fields, ocean velocity fields, ocean salinity and temperature fields, and ice thickness and concentration fields. The salinity field is practical salinity, and practical salinity is used throughout the article. Additional fields and computations, as presented in Section 2.2, can be reproduced using the OceanSpy v0.1

python package (Almansi et al., 2019). To avoid confusion with other datasets, we will refer to this simulation as MITgcm in the rest of the manuscript.

We used the Copernicus Climate Data Store Arctic Regional Reanalysis (CARRA on single levels) atmospheric reanalysis to put the wind conditions of the MITgcm year (September 2007–August 2008) in the context of a longer time series. The reanalysis data covers the period from 1998 to 2019 with a 3-hr temporal resolution and a 2.5 km spatial resolution, currently the best available time coverage with high resolution in the area. We also used the CARRA sea ice field, derived from two satellite sea ice concentration products: the European Space Agency Climate Change Initiative (ESA CCI) sea ice concentration product (SICCI; Toudal Pedersen et al., 2017), which has a 15–25 km resolution and is used whenever available, and the EUMETSAT OSISAF sea ice concentration product OSI-450 (Tonboe et al., 2016), which has a 30–60 km resolution and is used to fill gaps in the SICCI product.

We retrieved snapshots of the MODIS true color reflectance from the TERRA satellite at times of extreme wind events to investigate the sea ice response to extreme winds. The MODIS images have maximal resolution of 250 m, which allows detection of smaller details in sea ice behavior than with MITgcm and the satellite sea ice concentration product from CARRA, but good data is limited to satellite passes with clear skies.

2.2. Description of Methods

2.2.1. Definition and Detection of Wind Events

The wind analysis at Cape Farewell focuses on the region defined in Figure 1b, corresponding to the southernmost part of the east Greenland shelf, where strong winds are most likely to bring fresh surface waters to the Irminger Sea. Two main types of winds are dominant in that area; westerly winds and northeasterly winds (Figure 1c). We are interested in the extreme manifestation of those winds.

We identified the strongest events for both types of winds by using time series of spatially-averaged (within the box in Figure 1b) wind direction and speed in the area of interest. We defined tip jets as strong (>17 m s^{-1}), westerly winds (mean wind direction toward the 45°–135° quadrant with respect to north), lasting for more than 12 hr. Similarly, we defined strong northeasterly events as strong (>17 m s^{-1}) northeasterly winds (mean wind direction toward the 180°–270° quadrant with respect to north) lasting more than 12 hr. We considered two events of the same type to be part of the same event if occurring less than 12 hr apart.

Our identification method and chosen threshold are similar to the ones used in previous studies identifying extreme wind events near Greenland (Harden et al., 2011; Moore, 2012). The 17 m s^{-1} threshold corresponds to the 10% strongest westerly winds in the ASR-2 data of the MITgcm year, and to gale-force winds. The choice of other thresholds modify the number of detected events, but not the conclusions regarding the impact of strong wind events on the ocean at Cape Farewell. In this study, the mean winds in the area of interest at a given time are used to identify extreme wind events. Using maximum winds in the area rather than mean winds as done by Moore (2014) has the same effect as changing the threshold: It changes the number of detected events but not their characteristics nor the conclusions regarding their impact.

Though tip jets are the most likely to cause the strongest freshwater export at Cape Farewell, more moderate westerly winds are also likely to play a role. We identified moderate westerly winds using a similar criteria as for tip jets, but for wind speeds between 10 and 17 m s^{-1}.

2.2.2. Computation of Transports Across the Shelfbreak

We computed volume and freshwater transports across the shelfbreak at Cape Farewell, defined as the smoothed 800 m isobath (Figure 1b). The isobath is extracted from the ETOPO1 bathymetric data (NOAA, 2009) and smoothed with a 50 km window. Points along the shelfbreak are spaced 2–3 km apart.

We computed transports across each section of this line using the OceanSpy python toolbox (Almansi et al., 2019) "Survey" tool. Velocities at the shelfbreak are projected using the local shelf angle to compute the orthogonal velocity, which is then used to compute volume transport. Freshwater transport is computed with a reference practical salinity of 34.9, chosen because it is a good indication of the position of the salinity front and for consistency with previous studies. The cell thickness in MITgcm varies with depth. In order to make export values comparable at different depths, we computed the freshwater and volume transport per meter of the water column.

To compute across-shelf sea ice transport, we extracted sea ice velocities at the shelfbreak using the Survey tool, and projected them to obtain the orthogonal velocity. The sea ice volume transport is then computed as:

$$T_{ice} = v_{\perp ice} * H_{eff} * d_x \quad (1)$$

where $v_{\perp ice}$ (in m s^{-1}) is the ice velocity across the section, H_{eff} (in m) is the effective thickness of sea ice (thickness of the ice if it were homogeneously distributed over the cell) and d_x (in m) is the cell width. Freshwater transport across the shelfbreak due to snow is negligible.

In order to compare sea ice export to liquid freshwater export, we computed the freshwater transport equivalent of across-shelf sea ice export. Sea ice is not pure freshwater, so we first computed the liquid volume transport equivalent of sea ice transport, and then the freshwater transport equivalent as for liquid freshwater transport:

$$T_{ice/water} = T_{ice} * \frac{\rho_{ice}}{\rho_{water}} \quad (2)$$

$$T_{ice\_FWT} = T_{ice/water} * \left(\frac{S_{Ref} - \frac{S_{eff}}{H_{eff} * \rho_{ice}}}{S_{Ref}} \right) \quad (3)$$

with ρ_{water} = 1,027 kg m^{-3} is the density of seawater, ρ_{ice} = 917 kg m^{-3} is the density of ice, S_{Ref} is the reference salinity, and S_{eff} (g m^{-2}) the effective salinity, retrieved from MITgcm. The effective salinity in g m^{-2} corresponds to the amount of salt in grams in a given sea ice cell, and is thus divided by the effective thickness and the density of ice to obtain sea ice salinity.

Theoretical Ekman transport across the shelfbreak is computed using wind stress from MITgcm projected similarly along the shelfbreak as:

$$\begin{cases} T_{ekx} = \frac{\tau_y}{f * \rho_{water}} \\ T_{eky} = \frac{-\tau_x}{f * \rho_{water}} \end{cases} \quad (4)$$

with τ_x, τ_y being the horizontal wind stress components, and the Coriolis parameter $f = 10^{-4}$ s^{-1}.

2.2.3. Particle Release

To investigate the fate of freshwater during extreme wind events, we simulated numerical particle trajectories using MITgcm and the particle-tracking algorithm presented in Koszalka et al. (2013) and Gelderloos et al. (2016). Particles were released during 11 tip jets and 5 strong northeasterly wind events, every 6 hr, at all times identified as belonging to these events. The size of the ensemble of particle releases varied between 2 and 14 ensemble members, depending on the duration of the wind event. Each ensemble member contained 8,106 particles seeded between 0.5 and 100 m depth, at 0.5 km spacing along the smoothed 800-m isobath. Each ensemble member was run for 90 days. Since 90% of the particles took less than 7 days to reach the western side of Greenland, this is more than enough time for robust statistics.

Additionally, two sets of ensembles were run in 2D mode to mimic the behavior of floats in the real ocean, using only horizontal velocities. In the 2D simulations, particles were seeded at 0.5 and 15 m depth. The simulated trajectories in the 2D simulations were not significantly different from the 3D simulations, which gives us confidence that the pathways of real-life floats and simulated particles will be comparable. Since we are also interested in the vertical structure, we will discuss the 3D simulation results in this manuscript.

3. Extreme Wind Events at Cape Farewell

3.1. Identified Extreme Wind Events in MITgcm

Using the method presented in Section 2.2, we identified 11 tip jets and 5 strong northeasterly wind events during the MITgcm year. Figure 2 shows the time series of wind speed averaged over the area of interest (black line), with identified tip jets (red shade), and strong northeasterly (blue shade) events. In the MITgcm year, tip jets occur mainly in winter, from the end of October to early March, whereas the strong northeasterly events take

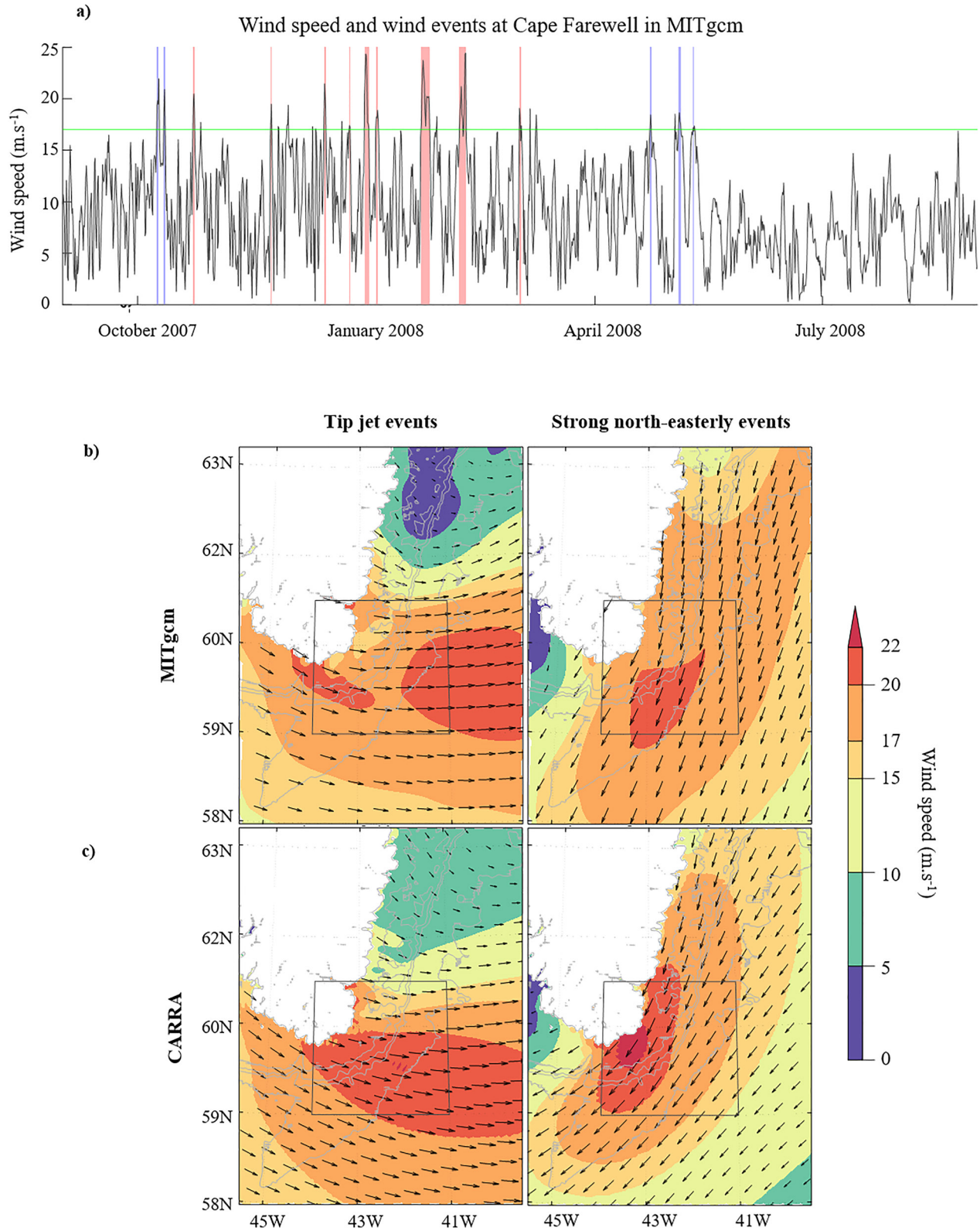

Figure 2. (a) Wind speed time series in the region of interest for MITgcm (black), detected tip jets (red shade), and northeasterly events (blue shade). The green line indicates the 17 m s^{-1} threshold value for extreme wind events. (b) Average wind speed and direction during tip jet and strong northeasterly events in MITgcm, from September 2007 to 2008. (c) Average wind speed and direction during tip jet and strong northeasterly events in CARRA, for the time period 1998–2019. Area of interest for wind time series shown in gray, isobaths in light gray: 200, 500, 1,000, and 2,000 m depth.

place outside of that period, in fall and spring. In the summer months (June–September), the mean wind is much weaker and no extreme events were identified.

The wind composite of identified tip jet events (Figure 2b) shows westerly winds extending offshore from Cape Farewell, with the strongest winds (>20 m s^{-1}) over the Irminger Sea, and only weak winds (<5 m s^{-1}) north of Cape Farewell. The wind composite of identified strong northeasterly events (Figure 2c) shows wind speeds between 15 and 20 m s^{-1} along the southeast shelf, and weak winds on the western side of Greenland. The structure and magnitude of these wind events is consistent with existing studies (Moore & Renfrew, 2005; Renfrew et al., 2009). Most detected events lasted between 0.5 and 1 day, with three exceptions during which gale force winds lasted two or 3 days. On average, the time evolution of tip jets shows a clear peak shape, with winds reaching 20 m s^{-1} at peak, from 10 m s^{-1} 30 hr before and after the peak. For northeasterlies, the curve is similar, but with stronger winds before the event and a weaker peak.

3.2. Comparison to Wind Events Identified in the 1998–2019 CARRA Time Series

We applied the same detection method to surface winds from the CARRA reanalysis, which spans 22 yr from 1998 to 2019. In total, we detected 240 tip jets and 289 strong northeasterly events during that period.

Characteristics of tip jet and strong northeasterly events are similar between CARRA and the ASR-2 reanalysis used in MITgcm, with a few differences. Northeasterly events are stronger in the CARRA reanalysis, and both tip jets and northeasterly events show strong winds closer to the coast in the CARRA reanalysis than in ASR-2 (Figures 2c and 2d). In CARRA, most events last between 0.5 and 1 day (183 tip jets and 205 northeasterly events), some events last between 1.5 and 2.5 days (50 tip jets and 70 northeasterly events) and only very few last for a longer time (less than 10 of each). Mean wind speeds in the area range mostly between 18 and 25 m s^{-1} with a long tail distribution of more extreme events up to 32 m s^{-1}, with similar magnitude for tip jets and strong northeasterlies.

The seasonal distribution of wind events in CARRA (not shown) is very similar to that in MITgcm: Most wind events are observed in the winter months, especially tip jets. A few strong northeasterly events are detected in summer, but most of them also take place in the winter months. In total, more than 90% of tip jets and 80% of strong northeasterlies take place between October and April. The composite of mean wind speeds in the area, centered on the peak wind of each event, shows a similar behavior as in MITgcm. The temporal evolution of wind speeds during tip jet and strong northeasterly events are here much more alike, with similar initial and peak speeds. The number of events varies from year to year (Figure 3), with a minimum of two tip jet events in the winter 2009–2010, and a maximum of 21 in 2014–2015. This year-to-year variability between the number of tip jets and northeasterly events is due to variability of background atmospheric conditions, that can be linked to the phase of the North Atlantic Oscillation (NAO, Hurrell, 1995), and in particular the position of the Icelandic low. During positive NAO phases, the North Atlantic storm track shifts northward, which favors conditions enabling tip jets, while during negative NAO phases the converse happens (Bakalian et al., 2007; Josey et al., 2019; Våge et al., 2009). This is visible in the correlation between the number of tip jets and the NAO index (Figure 3).

On average, we detected 11 tip jet events and 13 strong northeasterly events per year in CARRA. In the winter 2007–2008, 13 tip jet events and 12 strong northeasterly events were detected, close to the multiyear average. This makes 2007–2008 an adequate period to study the impact of wind events on freshwater export. As mentioned above, the mean wind speeds during strong northeasterlies are higher in CARRA than in MITgcm, which explains why more northeasterly events are identified as strong wind events in the reanalysis.

4. Impact on Liquid Freshwater Export

4.1. Export Across the Shelfbreak

The strong wind patterns presented in Section 3 can impact the top layer of the shelf waters. In particular, strong westerly winds, such as tip jets have the potential to drive freshwater export away from the shelf. To investigate this process, we defined the shelfbreak at Cape Farewell as the 800 m smoothed isobath, and then computed time series of volume and freshwater export across the shelfbreak as presented in Section 2.2. Figure 4 displays time series of volume, Ekman (as computed from Equation 4) and freshwater transport, all filtered with a 1-day

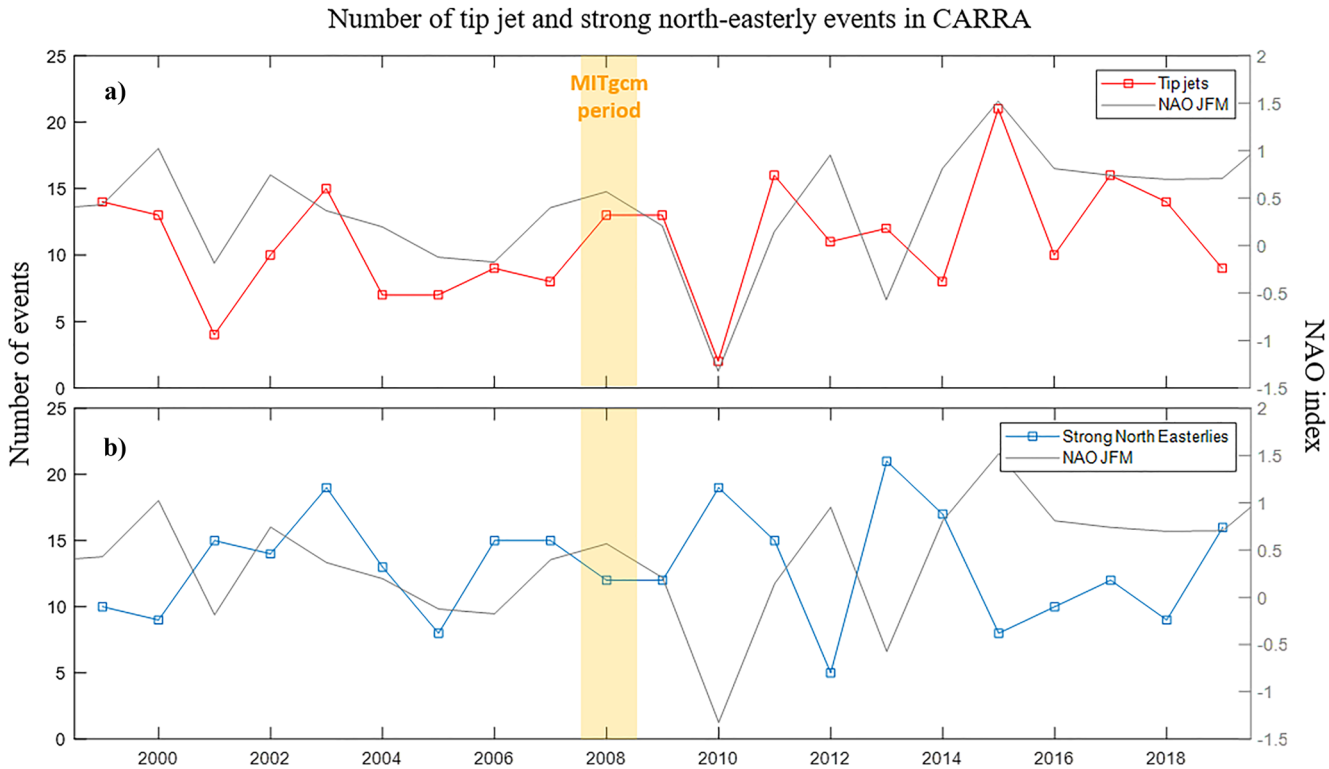

Figure 3. (a) Time series of number of tip jets per year in the CARRA reanalysis, and seasonal mean (January, February, and March) NAO index. (b) Time series of number of strong northeasterlies per year in the CARRA reanalysis, and seasonal mean (January, February, and March) NAO index; The number of wind events per year is computed from summer to summer so that the whole winter is included in the yearly means. The yellow area shows the period simulated in MITgcm.

low-pass second order Butterworth filter, together with identified tip jet events (dark gray shade) and moderate westerly wind events (light gray shade).

The time series of shelfbreak volume transport in the first 100 m, and Ekman transport show a strong correlation (Pearson's correlation coefficient >0.8), suggesting that export in the top layer of the water column is predominantly wind-driven (Figure 4a). Times identified as tip jets are associated with the strongest export at the shelfbreak. Moderate westerlies are also associated with export, though weaker.

Volume and freshwater transports across the shelfbreak are strongest at the surface, and surface export peaks occur both during tip jets and moderate westerlies (Figure 4b). At 25 m depth, only tip jets have a clear impact on volume and freshwater export (Figure 4c). The strongest wind and export events take place in winter, but moderate westerly events in summer can also lead to non-negligible freshwater export at the surface, especially due to fresher waters being present over the shelf in summer. For instance, a moderate westerly event on the 15th of August led to surface freshwater export comparable in intensity to the one happening on the 6th of February, associated with the most intense winter tip jet.

4.2. Salinity Changes During Different Wind Events

The previous section showed that westerly winds, and tip jets in particular, lead to freshwater export across the shelfbreak (defined as the 800 m isobath). To investigate in more detail what happens during these export events, we computed the salinity composites at the surface and along sections for tip jets, moderate westerlies, northeasterlies and weak winds (Figure 5). To avoid artifacts due to high seasonal variability in salinity and the temporally uneven distribution of tip jets compared to the other wind events, only the winter months are considered when computing the composites (December–April). Northeasterlies stronger than 10 m s^{-1} are used instead of the strong northeasterlies defined earlier due to the low number of such events detected in MITgcm during the winter months.

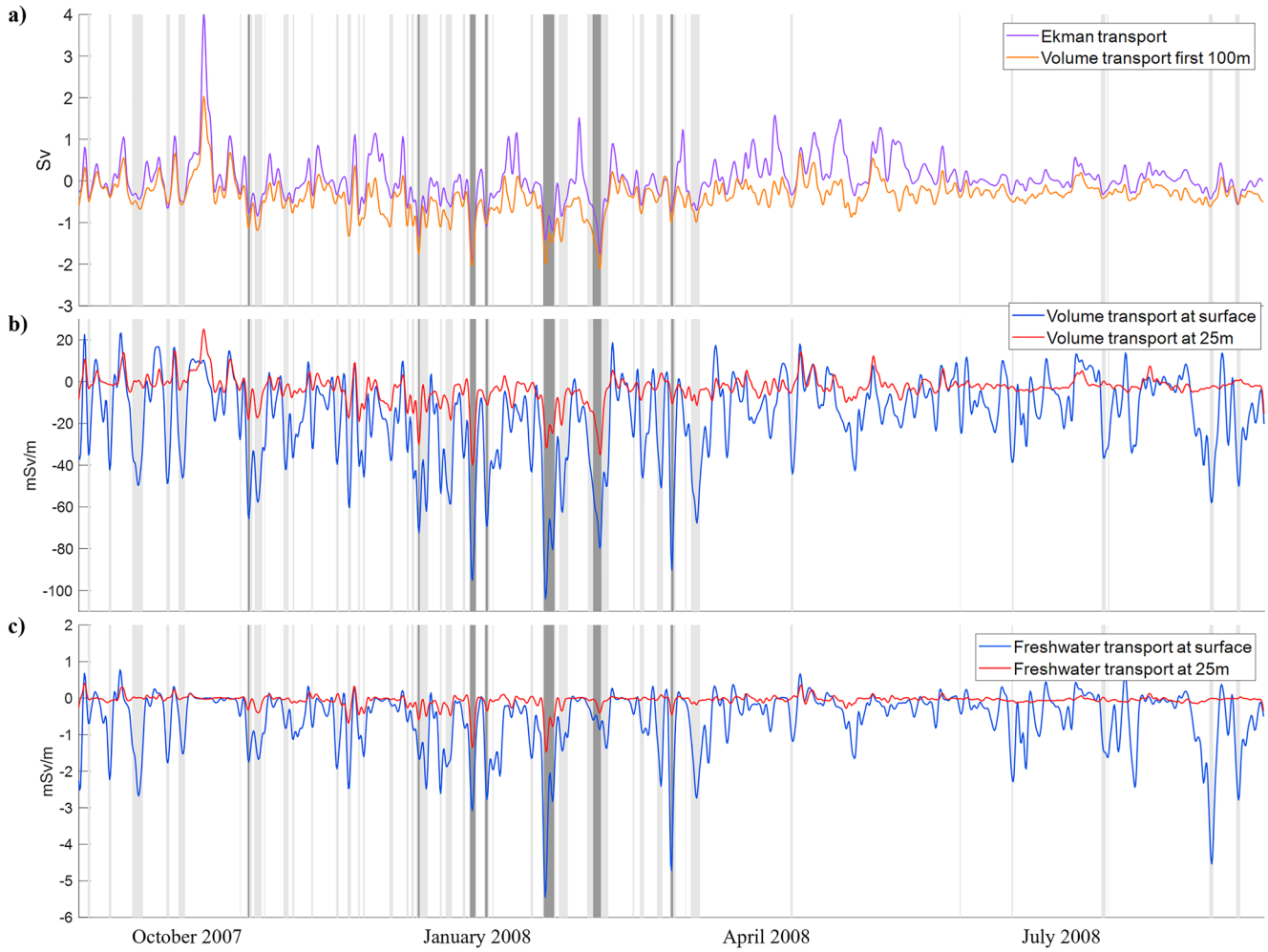

Figure 4. (a) Time series of Ekman transport (purple) and volume transport in the first 100 m (orange). (b) Time series of volume transport at the surface (blue) and 25 m (red). (c) Time series of freshwater transport at the surface (blue) and 25 m (red). Light gray lines correspond to moderate westerlies; dark gray lines to tip jets. All time series are filtered with a 1 day low-pass second order Butterworth filter.

During tip jets, fresher waters extend away from the coast south of Cape Farewell (Figure 5a). The 32.5 isohaline shows very fresh waters extending toward the shelfbreak, while the 34.9 isohaline shows that the salinity front situated at the shelfbreak moves slightly offshore. At Eirik Ridge, tip jets drive an extension of the fresher waters over the ridge. During northeasterly winds, the front moves in the opposite direction and fresher waters are brought closer to the coast than during weak winds.

Vertical sections of salinity composites (Figures 5b and 5c) show that tip jet events and, to a lesser extent, moderate westerlies, are associated with an offshore extension of fresh shelf waters. During tip jets, the extension is visible up to 100 m depth. In contrast, northeasterly events are associated with a vertical tilting of the isohalines compared to the weak-winds situation. This behavior is clearest for Section 2, which is located at Eirik Ridge, where most freshwater is exported during tip jet events.

4.3. Trajectories of Particles Released During Extreme Wind Events

The salinity composites show that strong wind events impact the EGC front at Eirik Ridge, with fresher waters in the upper 100 m pushed offshore during tip jets (Figure 5). This also agrees with the peaks in off-shelf freshwater transport in our time series presented in Figure 4. However, these analyses do not reveal whether freshwater is then exported to neighboring seas, or rejoins the EGC after the wind event. To further investigate where the freshwater goes during and after wind events, particles were released at the shelfbreak at all times identified as

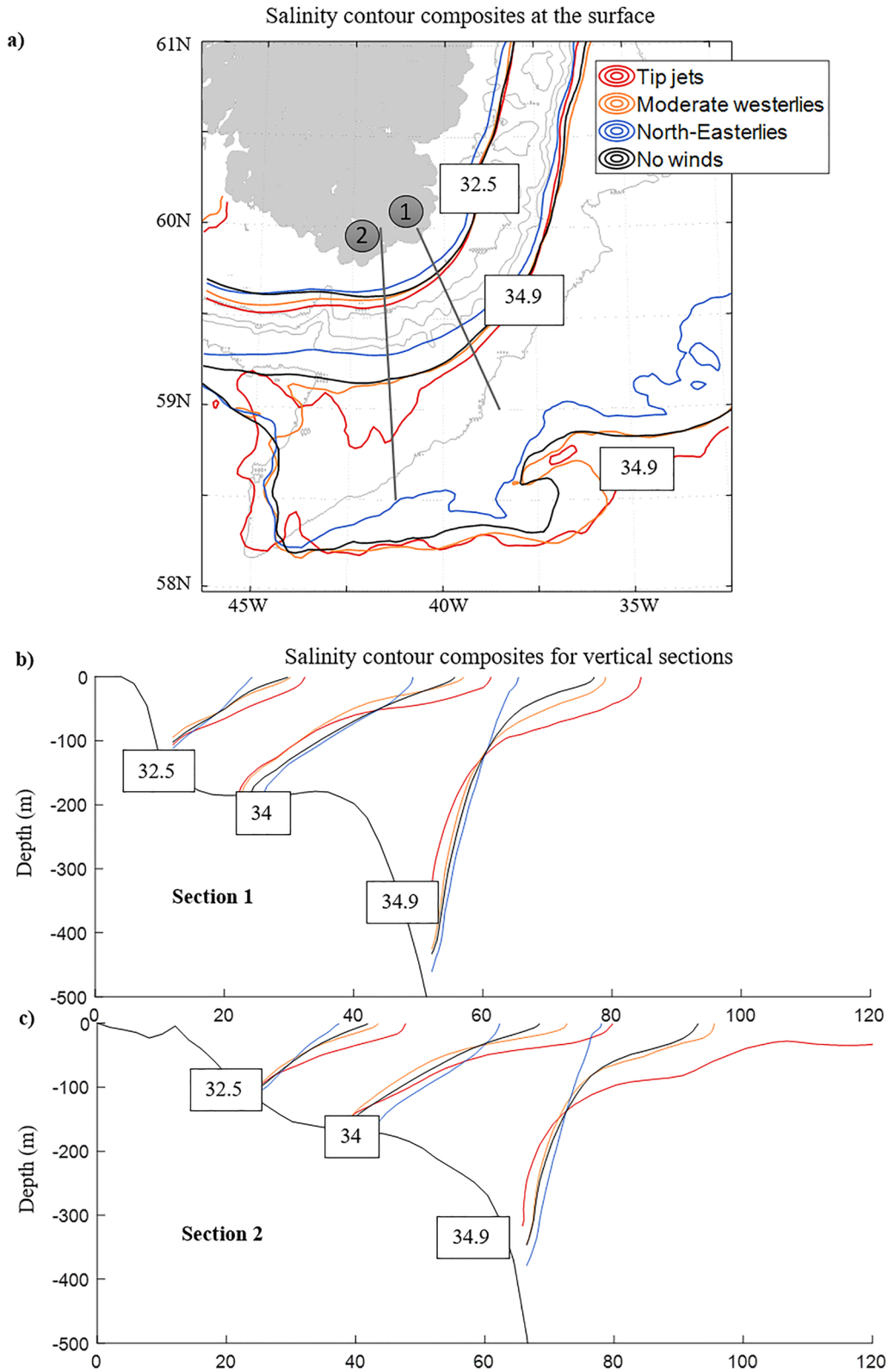

Figure 5. (a) Salinity composites at the surface. (b) Salinity composites along Section 1 on (a). (c) Same for Section 2. For composites, colors are: tip jets (red), moderate westerlies ≥10 m s^{-1} and <17 m s^{-1} (orange), northeasterlies ≥10 m s^{-1} (blue), and weak winds <10 m s^{-1} (black). Isobaths in gray for 200, 500, 1,000, and 2,000 m depth.

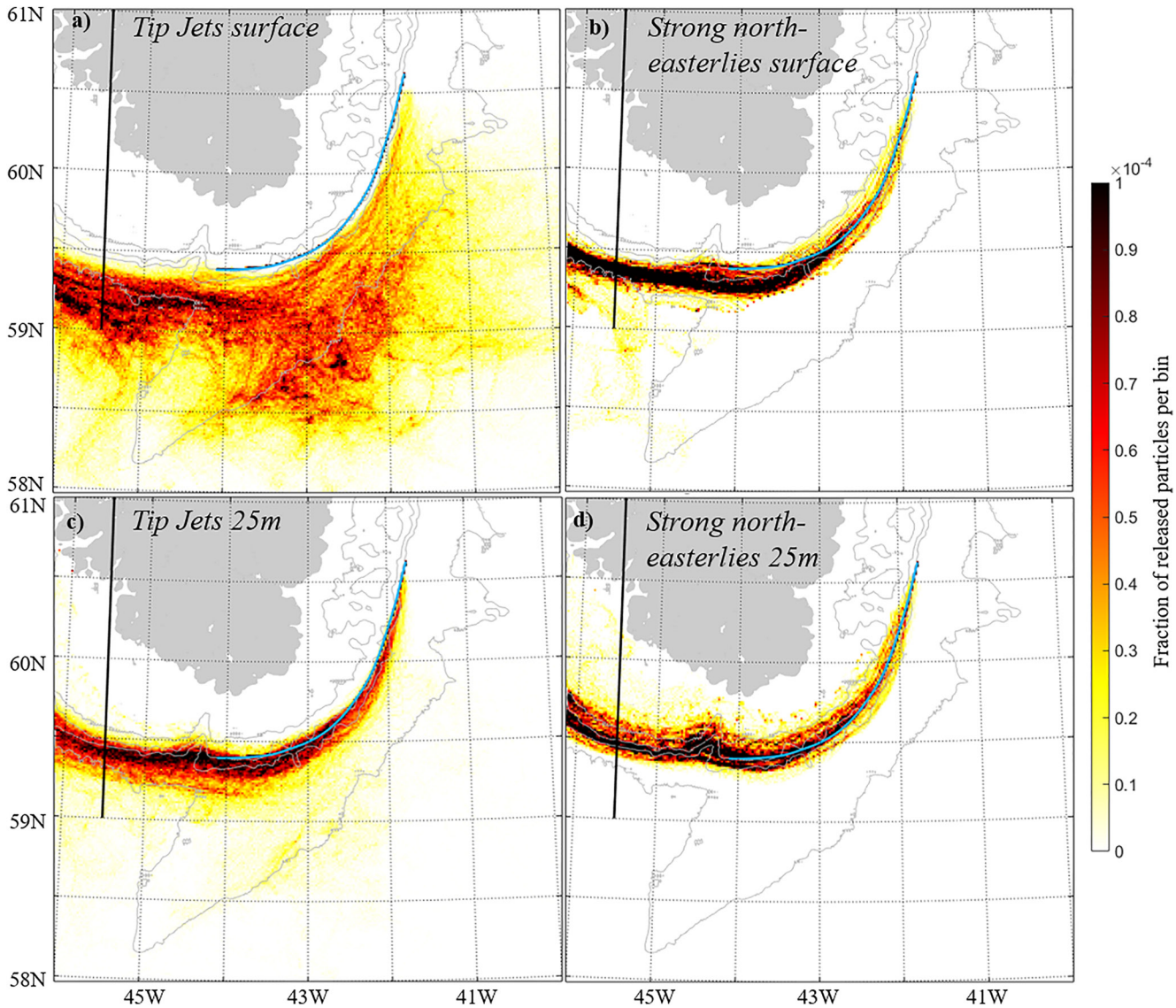

Figure 6. Density maps of particles within 2 weeks after release, with a bin size of 0.025° of longitude and 0.0125° latitude. The color bar corresponds to the fraction of released particles found in each bin. (a) Particles released at 0.5 m depth during tip jet events. (b) Particles released at 25 m depth during tip jet events. (c) Particles released at 0.5 m depth during strong northeasterly events. (d) Particles released at 25 m depth during strong northeasterly events. For all figures, the deployment line (blue) and the crossing line to the western side of Greenland (black) are shown. Isobaths in gray for 200, 500, 1,000, and 2,000 m depth.

part of tip jets and strong northeasterly wind events, as described in the methods Section 2.2.3. Density maps of particles within 2 weeks after their release are shown Figure 6.

Particles that were released at the shelfbreak during strong northeasterly events (Figures 6b and 6d) follow the shelfbreak toward the western side of Greenland. While the particles deployed at the surface tend to flow on the offshore side of the shelfbreak, the particles deployed at 25 m flow closer to the shelfbreak, and a few of them spread out onto the shelf. In the mean circulation, the direction of the shelfbreak current at 25 m is pointed slightly more inshore than the shelfbreak current at the surface. The salinity front between shelf and interior waters is also slanting toward the shore in the deeper layers, which could explain why particles deployed at 25 m more easily enter the shelf area.

Particles deployed during tip jets (Figures 6a and 6c) show a different behavior. Particles deployed at the surface are pushed offshore by the strong westerly winds. In the first 2 weeks after their release during tip jet events, these particles are found in the EGC, but also in the Western Irminger Sea and over Eirik Ridge. Particles released

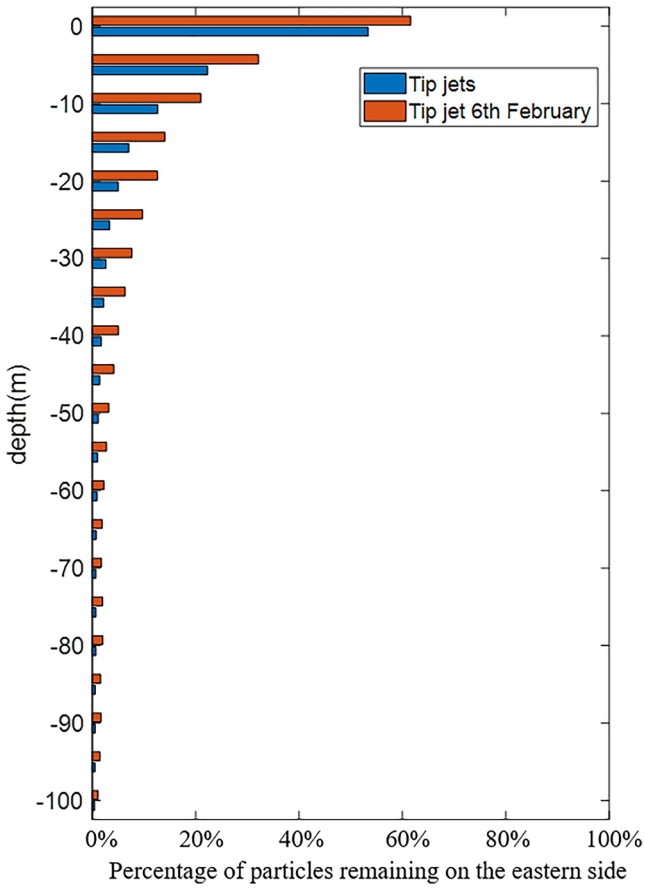

Figure 7. Fraction of particles that do not cross the 45.5°W, 59–61°N line to west Greenland within 2 weeks as a function of release depth, for particles released during all tip jet events, and particles released during the strongest tip jet identified in MITgcm, which started on the 6th of February.

at 25 m during tip jets mostly follow the shelfbreak into the West Greenland Current with only a few particles driven over Eirik Ridge, and nearly none exported to the Irminger Sea. Only the two most intense tip jet events (starting on the 22nd of January and the 6th of February) are associated with particle export at 25 m, which leads to the signal of export being fairly faint in the particle density distribution plot. This is consistent with the export time series presented in Figure 4, which show that strong export at 25 m depth only occurs during the most intense and longest tip jet events. In Figure 4a–4c, we see particles coming back to the region after they crossed the MITgcm western boundary. This recirculation is also visible in the mean surface circulation in MITgcm, and is therefore not due to wind events. It could be related to a previously identified recirculation in the area (Fischer et al., 2018), but this is beyond the scope of this study. Furthermore, because it takes place so close to the boundary, this setup of the MITgcm is not adapted to investigate it.

To quantify the fraction of particles exported during each type of wind event, we computed the number of particles crossing the 45.5°W line to west Greenland in the range 59°–61°N (black line Figure 6), as a function of release depth. During strong northeasterly events, all particles crossed that line within 2 weeks (<1% of the particles released at the surface stayed on the eastern side of Greenland). During tip jet events, the number of particles staying on the eastern side of Greenland depended on the depth at which they were released, but also on the intensity of the tip jet event. About 47% of the particles released at the surface did not cross the line to west Greenland within 2 weeks (Figure 7), meaning they were exported to the Irminger Sea or driven over Eirik Ridge. The percentage of exported particles decreases with the release depth to 18% for 5 m, 10% for 10 m, and only 3% for 25 m. The same analysis is made for the most intense tip jet event, taking place from the 6th to the 9th of February (in red on Figure 7). About 53% of the particles released at the surface during that event did not cross the line to west Greenland, 25% at 5 m, down to 16% at 10 m, and 7% at 25 m. More particles are exported at the surface during this strong event, and the fraction of particles exported decreases more slowly with depth than for the ensemble of tip jet events.

5. Wind-Driven Solid Freshwater Export

5.1. Wind-Driven Ice Export in MITgcm

Strong wind events at Cape Farewell are likely to impact not only liquid freshwater export but also sea ice cover, and lead to export of sea ice that then melts in the Irminger Sea. To evaluate the impact of westerlies on ice export at Cape Farewell, the freshwater equivalent of sea ice transport across the shelfbreak is computed from MITgcm using Equations 1–3. Figure 8a shows the resulting across-shelf transport together with identified tip jet (red) and moderate westerly (light red) events. Some sea ice export events seem associated with wind events, such as the moderate westerlies of mid-January and late February; however, tip jets are not associated with the strongest export, and there is no clear correlation between sea ice export and the intensity of westerly winds. Ice cover at Cape Farewell is highly variable throughout the winter and, in general, ice concentration is very low in the area (blue line in Figure 8a). It is therefore likely that, even if sea ice responds to westerly wind events by veering eastwards, it does not reach the shelfbreak, and computed export depends as much on how much sea ice is present at the time of the wind event as on the wind event itself.

We investigated the impact of tip jets on sea ice cover in MITgcm using sea ice composites at the peak of each wind event, 24 hr before and 24 hr after (Figure 8b). Tip jet events are considered only if ice concentration is above 5% in the area of interest 24 hr before peak winds. As westerly winds increase, the sea ice moves away from the coast and toward the Irminger Sea. Overall, ice concentrations decrease significantly south of 61°N during the wind event. As the wind calms down, very low concentrations of sea ice re-enter the shelf. The decrease in

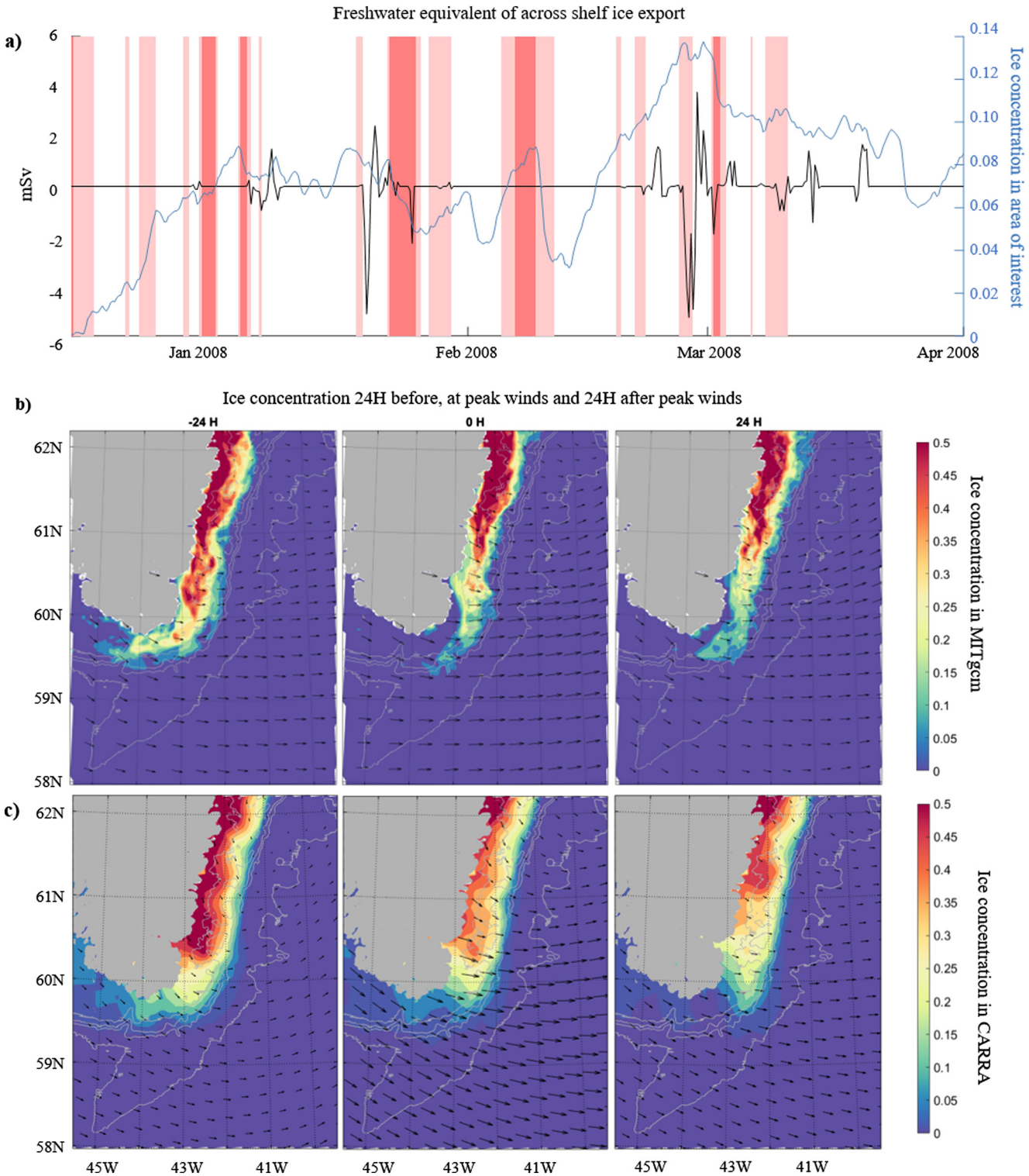

Figure 8. (a) Time series of sea ice freshwater equivalent transport (black) and sea ice concentration (blue) in the area of interest. Tip jet events are indicated in red and moderate westerlies in light red. Negative transport is directed off-shelf. (b) Composite of ice concentration and 10 m winds from MITgcm during tip jet events, 24 hr before, during, and 24 hr after peak tip jet winds. (c) Composite of ice concentration and 10 m winds from CARRA during tip jet events, 24hr before, during, and 24 hr after peak tip jet winds. Isobaths in gray for 200, 500, 1,000, and 2,000 m depth.

sea ice concentration is likely due to enhanced melting past the front as the ice enters the warmer waters offshore. Even though the response of sea ice to tip jets is clear, the ice only rarely crosses the shelfbreak, which could also contribute to the low level of ice export and lack of correlation with wind events mentioned above.

5.2. Effect of Tip Jets on Sea Ice in CARRA

To investigate the impact of westerlies on sea ice at Cape Farewell over a longer time period, we apply the same analysis to the CARRA sea ice concentration data that are derived from satellite observations (Figure 8c). As for the analysis presented above, wind events are only considered if ice concentration is above 5% in the area of interest 24 hr before peak wind. This corresponds to 19 tip jets, less than 10% of all tip jets detected in CARRA.

The results are similar to those we obtained with MITgcm, although the satellite products used in the CARRA reanalysis for sea ice have a lower resolution (15–60 km depending on conditions and what product can be used). During tip jets, ice concentration decreases close to the coast, and sea ice at Cape Farewell detaches from the coast to form a tongue along the shelfbreak. A general reduction in sea ice concentrations is seen south of 61°N indicating a loss of ice on the shelf. Similar to the MITgcm results, the ice stays mostly confined over the shelf even though it veers eastwards as a response to tip jets.

5.3. Sea Ice Response to Tip Jets as Seen With MODIS

Tip jet events lead to a decrease in sea ice cover at Cape Farewell in both the MITgcm simulation and the satellite derived sea ice product retrieved from the CARRA reanalysis. However, sea ice remains mostly on the shelf, even as it turns eastward in response to wind forcing. This leads to only a few occurrences of across-shelf sea ice export throughout the year. We used snapshots from the MODIS true-color imagery at Cape Farewell to investigate whether this result is consistent with higher resolution observations (Figure 9). The snapshots correspond to the tip jet events starting on the 28th of January and on the 6th of February, which were detected in both the ASR-2 reanalysis used in MITgcm, and in CARRA, and selected based on ice cover and the absence of clouds.

The MODIS snapshots show sea ice responding in a similar way as outlined earlier, but also reveal details that were not visible in MITgcm and the satellite sea ice concentration products from CARRA. During both tip jet events, sea ice is pushed away from the coast, forming a tongue at Cape Farewell that fans out into the Irminger Sea. On the day following the strongest winds the sea ice is further dispersed, broken up into smaller pieces and much less concentrated, likely melting as it enters the warmer waters in the Irminger Sea. The bathymetry shows that the ice extends further off the shelfbreak than in all the export events investigated in MITgcm, suggesting that the model-based export might be an underestimate.

6. Discussion and Conclusions

Using results from a high-resolution model, we showed that strong westerly winds at Cape Farewell can impact the water column up to 100 m deep and lead to tilting of the front and an offshore extension of the fresh water layer (Figure 5), with part of the surface waters exported off the shelf, over Eirik Ridge and into the Irminger Sea (Figure 6). We are interested in whether such liquid freshwater export is significant and could impact regional convection and overturning. At the latitude of Cape Farewell the EGC in MITgcm has a yearly mean freshwater transport of 160 mSv in the upper 100 m (computed across Section 1 in Figure 5a). This freshwater transport reaches 200 mSv during tip jets as the EGC is speeding up due to the enhanced wind forcing. On average, tip jet events lead to the export of 37.5 mSv of freshwater at the shelfbreak in the first 100 m, nearly one fifth of the upper EGC transport. Tip jets are associated with the strongest freshwater export at Cape Farewell, but moderate westerlies are much more frequent and can also drive offshore export at the very surface (Figure 4c). On average, 15.9 mSv of freshwater was exported during moderate westerlies, amounting to a total of 78.4 km^3 of freshwater exported during moderate westerlies of the MITgcm year, compared with 38 km^3 during tip jet events. While tip jets only take place during the winter months, moderate westerlies also occur in summer, when the shelf is particularly fresh, which leads to significant freshwater export during the summer months. Though most export occurred in winter, August was the third month with most freshwater export (11.8% of the total export), and in total, 37.8% of the annual freshwater export across the shelfbreak took place from May to October. Such wind-driven freshwater export at Cape Farewell in summer could enhance re-stratification processes and impact

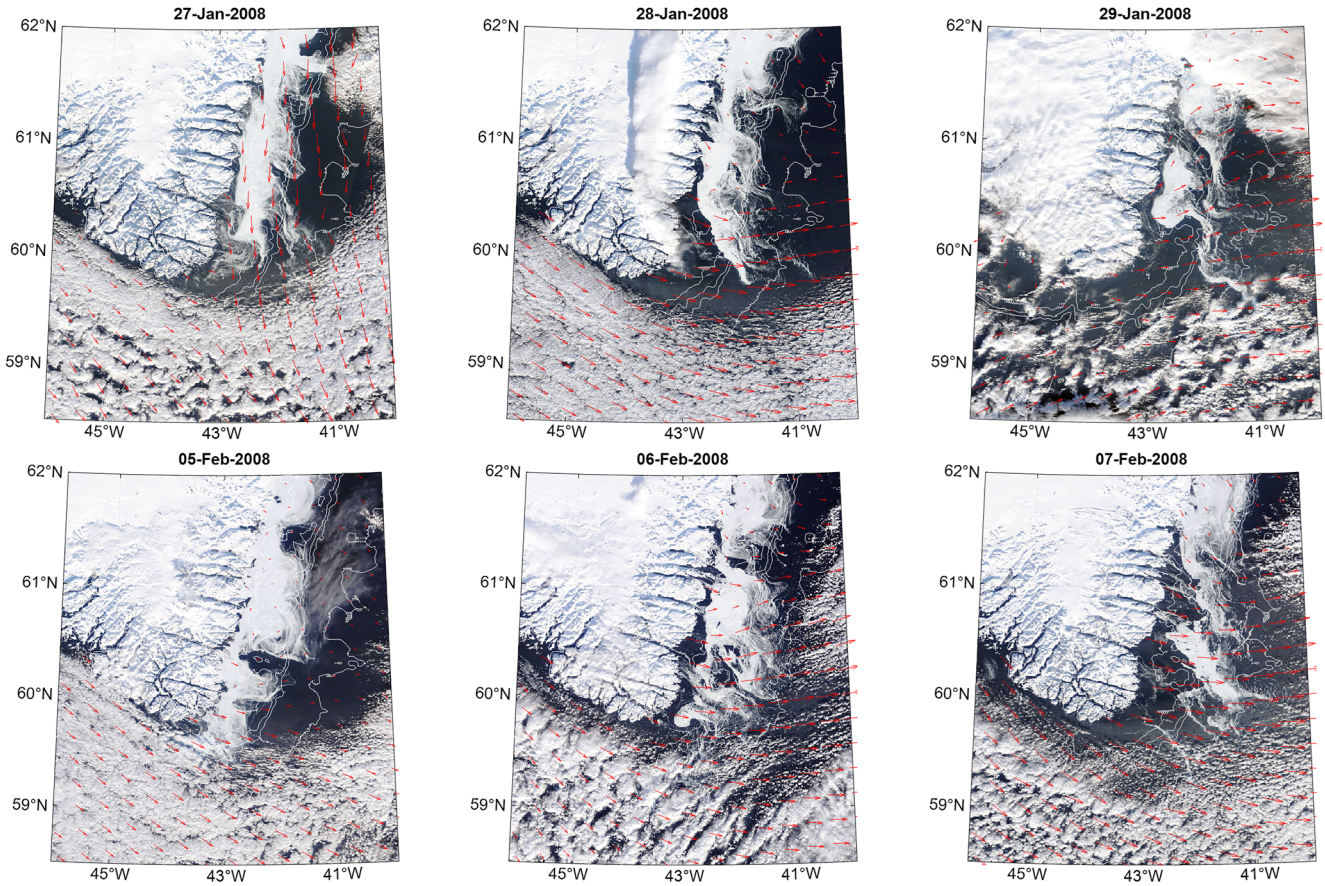

Figure 9. MODIS imagery during the strong wind events taking place around 28th of January and 6th of February. Isobaths in white for 200, 500, 1,000, and 2,000 m depth. CARRA 10 m winds are shown in red.

the pre-conditioning for deep convection (Oltmans et al., 2018). However, the particle deployment and salinity composites showed that freshwater is brought the furthest offshore during the strongest wind events, which suggests that, although moderate westerly winds can lead to export at the shelfbreak, tip jets are likely to be more important for export to deep convection regions.

Strong wind events at Cape Farewell also impact the sea ice cover, but we find that they only lead to minimal sea ice export at the shelfbreak (Figure 8). Impact of strong wind events on sea ice cover along the Greenland shelf elsewhere has previously been investigated by Oltmanns et al. (2014), who found that katabatic winds in the coastal region around Sermilik Fjord lead to a strong decrease (29%) of ice cover in Sermilik Trough. Both in MITgcm and the satellite products of the CARRA reanalysis, tip jets are associated with an eastward shift and a decrease of sea ice concentration at Cape Farewell, with sea ice remaining on the shelf, or disappearing as it reaches the shelfbreak. In MITgcm, sea ice export at the shelfbreak is not well correlated to wind events and is three orders of magnitude smaller than liquid freshwater export (annual volume of freshwater exported, with a reference salinity of 34.9: 0.305 km^3 for sea ice, against 207 km^3 for liquid freshwater in the first 100 m). This could be explained by the intermittent sea ice cover at Cape Farewell: most of the tip jets and westerly events take place at times when there is not enough ice to lead to export. The MODIS imagery snapshots show that tip jets can lead to sea ice tongues crossing the shelfbreak, which we never see in either MITgcm or CARRA, even during the strongest events. MODIS shows that the sea ice brought offshore during these events is broken up and forms fine filaments, which could explain why it is not resolved in the other data sets, which have a lower resolution. However, even though the MODIS observations suggest an underestimation of sea ice export in MITgcm, the filaments and broken-up ice tongues that are not resolved in the model only represent a small amount of freshwater, and the actual ice export is still likely to be much smaller than the liquid export.

Deep convection in the Irminger Sea takes place in the central Irminger Gyre (de Jong & de Steur, 2016; Våge et al., 2011) and south of Cape Farewell (De Jong et al., 2012; Piron et al., 2016, 2017). Particle tracking showed that a portion of surface waters exported across the shelfbreak during tip jet events can reach these two regions, but such export is limited to the strongest events. A recent study by Le Bras et al. (2020) showed convection up to 750 m at the edge of the EGC that forms lighter, shallower convective waters, that enter the Deep Western Boundary Current more easily. The outward tilting of the EGC front, observed during tip jets but also, to a lesser extent, during moderate westerlies, locally strengthens stratification where these waters are formed and may thereby affect the strength of near-boundary convection. When (shallow) convection does occur, the freshwater will be incorporated into the mixed layers, affecting the properties of the convectively formed water. This can also contribute to the lower salinities observed in mixed layers south of Cape Farewell compared to the central Irminger Sea, a signal which is subsequently transported to the central Irminger Sea at mid-depth (de Jong et al., 2012). A smaller amount of freshwater is likely to enter the central Irminger Sea along the surface and will similarly affect stratification and properties of convective water there.

In this study, we identified the importance of tip jet events in driving liquid freshwater off the shelf, and potentially toward convection regions. There is a strong interannual variability in the number of tip jet events, which is linked to background synoptic conditions and in particular the NAO phase (Bakalian et al., 2007; Våge et al., 2009). Years with high NAO phase and numerous tip jet events have been linked to particularly deep convection in the Irminger Sea as well as particularly fresh vintages of convective water (Van Aken et al., 2011), which suggests that current levels of freshwater export at Cape Farewell do not immediately inhibit convection, but could influence its strength and the properties of the convectively formed water masses. Whether this balance will be disrupted with increases in freshwater transport in the EGC linked to Greenland ice sheet melt and Arctic freshwater export is a subject for future studies.

Data Availability Statement

The MITgcm numerical solutions used in this study are available on SciServer (http://sciserver.org), developed by the Institute for Data Intensive Engineering and Science at Johns Hopkins University. Instructions for accessing the dataset can be found at: https://oceanspy.readthedocs.io/en/latest/datasets.html. The CARRA reanalysis data is available on the Copernicus Climate Data Store (https://cds.climate.copernicus.eu/). The MODIS data is available from the NASA worldview snapshots tool (https://wvs.earthdata.nasa.gov/). The NAO index is available from NOAA climate prediction center (https://www.cpc.ncep.noaa.gov/products/precip/CWlink/pna/nao.shtml). The topography is extracted from the NOAA ETOPO1 product (https://doi.org/10.7289/V5C8276M).

Acknowledgments
We thank the reviewers and editor for their comments, which improved the overall quality of the article. This project is financially supported by the Innovational Research Incentives Scheme of the Netherlands Organisation for Scientific Research (NWO) under grant agreement no. 016.Vidi.189.130. Renske Gelderloos is financially supported by the U.S. National Science Foundation under Grant OCE-2048496.

References

Aagaard, K., & Carmack, E. C. (1989). The role of sea ice and other fresh water in the Arctic circulation. *Journal of Geophysical Research*, *94*(C10), 14485. https://doi.org/10.1029/JC094iC10p14485

Almansi, M., Gelderloos, R., Haine, T. W. N., Saberi, A., & Siddiqui, A. H. (2019). OceanSpy: A Python package to facilitate ocean model data analysis and visualization. *Journal of Open Source Software*, *4*(39), 1506. https://doi.org/10.21105/joss.01506

Almansi, M., Haine, T. W. N., Gelderloos, R., & Pickart, R. S. (2020). Evolution of Denmark Strait overflow cyclones and their relationship to overflow surges. *Geophysical Research Letters*, *47*, e2019GL086759. https://doi.org/10.1029/2019GL086759

Almansi, M., Haine, T. W. N., Pickart, R. S., Magaldi, M. G., Gelderloos, R., & Mastropole, D. (2017). High-frequency variability in the circulation and hydrography of the Denmark Strait overflow from a high-resolution numerical model. *Journal of Physical Oceanography*, *47*(12), 2999–3013. https://doi.org/10.1175/JPO-D-17-0129.1

Bacon, S., Marshall, A., Holliday, N. P., Aksenov, Y., & Dye, S. R. (2014). Seasonal variability of the East Greenland Coastal Current. *Journal of Geophysical Research: Oceans*, *119*(6), 3967–3987. https://doi.org/10.1002/2013JC009279

Bakalian, F., Hameed, S., & Pickart, R. (2007). Influence of the Icelandic Low latitude on the frequency of Greenland tip jet events: Implications for Irminger Sea convection. *Journal of Geophysical Research: Oceans*, *112*, C04020. https://doi.org/10.1029/2006JC003807

Bakker, P., Schmittner, A., Lenaerts, J. T. M., Abe-Ouchi, A., Bi, D., van den Broeke, M. R., et al. (2016). Fate of the Atlantic Meridional Overturning Circulation: Strong decline under continued warming and Greenland melting. *Geophysical Research Letters*, *43*(23), 12252–12260. https://doi.org/10.1002/2016GL070457

Bamber, J. L., Tedstone, A. J., King, M. D., Howat, I. M., Enderlin, E. M., van den Broeke, M. R., & Noel, B. (2018). Land ice freshwater budget of the Arctic and North Atlantic Oceans: 1. Data, methods, and results. *Journal of Geophysical Research: Oceans*, *123*(3), 1827–1837. https://doi.org/10.1002/2017JC013605

Böning, C. W., Behrens, E., Biastoch, A., Getzlaff, K., & Bamber, J. L. (2016). Emerging impact of Greenland meltwater on deepwater formation in the North Atlantic Ocean. *Nature Geoscience*, *9*(7), 523–527. https://doi.org/10.1038/ngeo2740

Bromwich, D. H., Wilson, A. B., Bai, L., Liu, Z., Barlage, M., Shih, C.-F., et al. (2018). The Arctic system reanalysis, version 2. *Bulletin of the American Meteorological Society*, *99*(4), 805–828. https://doi.org/10.1175/BAMS-D-16-0215.1

Buckley, M. W., & Marshall, J. (2016). Observations, inferences, and mechanisms of the Atlantic Meridional Overturning Circulation: A review. *Reviews of Geophysics*, *54*, 5–63. https://doi.org/10.1002/2015RG000493

Collins, M. (2019). Extremes, abrupt changes and managing risks. In H.-O. Pörtner, D. C. Roberts, V. Masson-Delmotte, P. Zhai, M. Tignor, E. Poloczanska, et al. (Eds.), *IPCC special report on the ocean and cryosphere in a changing climate* (pp. 589–655). Intergovernmental Panel on Climate Change.

de Jong, M. F., Oltmanns, M., Karstensen, J., & de Steur, L. (2018). Deep convection in the Irminger Sea observed with a dense mooring array. *Oceanography*, *31*(1), 50–59. https://doi.org/10.5670/oceanog.2018.109

de Jong, M. F., & De Steur, L. (2016). Strong winter cooling over the Irminger Sea in winter 2014-2015, exceptional deep convection, and the emergence of anomalously low SST. *Geophysical Research Letters*, *43*, 7106–7113. https://doi.org/10.1002/2016GL069596

de Jong, M. F., Van Aken, H. M., Våge, K., & Pickart, R. S. (2012). Convective mixing in the central Irminger Sea: 2002-2010. *Deep-Sea Research Part I: Oceanographic Research Papers*, *63*, 36–51. https://doi.org/10.1016/j.dsr.2012.01.003

Dickson, R. R., Meincke, J., Malmberg, S., & Lee, A. J. (1988). The "great salinity anomaly" in the northern North Atlantic 1968–1982. *Progress in Oceanography*, *20*, 103–151. https://doi.org/10.1016/0079-6611(88)90049-3

Dodd, P. A., Heywood, K. J., Meredith, M. P., Naveira-Garabato, A. C., Marca, A. D., & Falkner, K. K. (2009). Sources and fate of freshwater exported in the East Greenland Current. *Geophysical Research Letters*, *36*, L19608. https://doi.org/10.1029/2009gl039663

Doyle, J. D., & Shapiro, M. A. (1999). Flow response to large-scale topography: The Greenland tip jet. *Tellus*, *51A*, 728–748. https://doi.org/10.1034/j.1600-0870.1996.00014.x

Dukhovskoy, D. S., Myers, P. G., Platov, G., Timmermans, M.-L., Curry, B., Proshutinsky, A., et al. (2016). Greenland freshwater pathways in the sub-Arctic Seas from model experiments with passive tracers. *Journal of Geophysical Research: Oceans*, *121*, 877–907. https://doi.org/10.1002/2015JC011290

Duyck, E., & de Jong, M. F. (2021). Circulation over the south-east Greenland shelf and potential for liquid freshwater export: A drifter study. *Geophysical Research Letters*, *48*. https://doi.org/10.1029/2020GL091948

Fischer, J., Karstensen, J., Oltmanns, M., & Schmidtko, S. (2018). Mean circulation and EKE distribution in the Labrador Sea water level of the subpolar North Atlantic. *Ocean Science*, *14*, 1167–1183. https://doi.org/10.5194/os-14-1167-2018

Foukal, N. P., Gelderloos, R., & Pickart, R. S. (2020). A continuous pathway for fresh water along the East Greenland shelf. *Science Advances*, *6*, eabc4254. https://doi.org/10.1126/sciadv.abc4254

Gelderloos, R., Straneo, F., & Katsman, C. A. (2012). Mechanisms behind the temporary shutdown of deep convection in the Labrador Sea: Lessons from the great salinity anomaly years 1968–71. *Journal of Climate*, *25*(19), 6743–6755. https://doi.org/10.1175/JCLI-D-11-00549.1

Gelderloos, R., Szalay, A. S., Haine, T. W. N., & Lemson, G. (2016). A fast algorithm for neutrally-buoyant Lagrangian particles in numerical ocean modeling. In *Proceedings of the 2016 IEEE 12th International Conference on e-Science*(pp. 381–388). Institute of Electrical and Electronics Engineers. https://doi.org/10.1109/eScience.2016.7870923

Haine, T. W. N., Curry, B., Gerdes, R., Hansen, E., Karcher, M., Lee, C., et al. (2015). Arctic freshwater export: Status, mechanisms, and prospects. *Global and Planetary Change*, *125*, 13–35. https://doi.org/10.1016/j.gloplacha.2014.11.013

Harden, B. E., Renfrew, I. A., & Petersen, G. N. (2011). A climatology of wintertime barrier winds off southeast Greenland. *Journal of Climate*, *24*, 4701–4717. https://doi.org/10.1175/2011JCLI4113.1

Hátún, H., Eriksen, C. C., & Rhines, P. B. (2007). Buoyant eddies entering the Labrador Sea observed with gliders and altimetry. *Journal of Physical Oceanography*, *37*, 2838–2854. https://doi.org/10.1175/2007JPO3567.1

Håvik, L., Pickart, R. S., Torres, D. J., Thurnherr, A. M., Beszczynska-Möller, A., Walczowki, W., et al. (2017). Evolution of the east Greenland Current from fram strait to Denmark strait: Synoptic measurements from summer 2012. *Journal of Geophysical Research: Oceans*, *122*, 1974–1994. https://doi.org/10.1002/2016JC012228

Hurrell, J. W. (1995). Decadal trends in the North Atlantic Oscillation: Regional temperatures and precipitation. *Science*, *269*, 676–679. https://doi.org/10.1126/science.269.5224.676

Josey, S. A., de Jong, M. F., Oltmanns, M., Moore, G. K., & Weller, R. A. (2019). Extreme variability in Irminger Sea winter heat loss revealed by ocean observatories initiative mooring and the ERA5 reanalysis. *Geophysical Research Letters*, *46*, 293–302. https://doi.org/10.1029/2018GL080956

Koszalka, I. M., Haine, T. W. N., & Magaldi, M. G. (2013). Fates and travel times of Denmark Strait overflow water in the Irminger Basin. *Journal of Physical Oceanography*, *43*, 2611–2628. https://doi.org/10.1175/JPO-D-13-023.1

Le Bras, I. A.-A., Straneo, F., Holte, J., & Holliday, N. P. (2018). Seasonality of freshwater in the East Greenland Current System from 2014 to 2016. *Journal of Geophysical Research: Oceans*, *123*(12), 8828–8848. https://doi.org/10.1029/2018JC014511

Le Bras, I. A.-A., Straneo, F., Holte, J., Jong, M. F., & Holliday, N. P. (2020). Rapid export of waters formed by convection near the Irminger Sea's Western Boundary. *Geophysical Research Letters*, *47*(3), e2019GL085989. https://doi.org/10.1029/2019GL085989

Li, F., Lozier, M. S., Bacon, S., Bower, A., Cunningham, S. A., de Jong, M. F., et al. (2021). Subpolar North Atlantic Western Boundary density anomalies and the meridional overturning circulation. *Nature Communications*, *12*(2021), 3002. https://doi.org/10.1038/s41467-021-23350-2

Lilly, J. M., Rhines, P. B., Schott, F., Lavender, K., Lazier, J., Send, U., & D'Asaro, E. (2003). Observations of the Labrador Sea eddy field. *Progress in Oceanography*, *59*, 75–176. https://doi.org/10.1016/J.POCEAN.2003.08.013

Lozier, M. S., Li, F., Bacon, S., Bahr, F., Bower, A. S., Cunningham, S. A., et al. (2019). A sea change in our view of overturning in the subpolar North Atlantic. *Science*, *363*(6426), 516–521. https://doi.org/10.1126/science.aau6592

Manabe, S., & Stouffer, R. (1995). Simulation of abrupt climate change induced by freshwater input to the North Atlantic Ocean. *Nature*, *378*, 165–167. https://doi.org/10.1038/378165a0

Marshall, J., Adcroft, A., Hill, C., Perelman, L., & Heisey, C. (1997). A finite-volume, incompressible Navier Stokes model for studies of the ocean on parallel computers. *Journal of Geophysical Research*, *102*(C3), 5753–5766. https://doi.org/10.1029/96JC02775

Medvedev, D., Lemson, G., & Rippin, M. (2016). Sciserver compute: Bringing analysis close to the data. *Proceedings of the 28th international conference on scientific and statistical database management, SSDBM'16* (pp. 271–274). Association for Computing Machinery. https://doi.org/10.1145/2949689.2949700

Moore, G. W. K. (2003). Gale force winds over the Irminger Sea to the East of Cape Farewell, Greenland. *Geophysical Research Letters*, *30*(17), 1894. https://doi.org/10.1029/2003GL018012

Moore, G. W. K. (2012). A new look at Greenland flow distortion and its impact on barrier flow, tip jets and coastal oceanography. *Geophysical Research Letters*, *39*, L22806. https://doi.org/10.1029/2012GL054017

Moore, G. W. K. (2014). Mesoscale structure of Cape Farewell tip jets. *Journal of Climate*, *27*(23), 8956–8965. https://doi.org/10.1175/JCLI-D-14-00299.1

Moore, G. W. K., & Renfrew, I. A. (2005). Tip jets and barrier winds: A QuikSCAT climatology of high wind speed events around Greenland. *Journal of Climate*, *18*(18), 3713–3725. https://doi.org/10.1175/JCLI3455.1

National Oceanic and Atmospheric Administration (NOAA) National Geophysical Data Center. (2009). *ETOPO1 1 arc minute global relief model*. National Oceanic and Atmospheric Administration National Centers for Environmental Information. https://doi.org/10.7289/V5C8276M

Oltmanns, M., Karstensen, J., & Fischer, J. (2018). Increased risk of a shutdown of ocean convection posed by warm North Atlantic summers. *Nature Climate Change*, *8*, 300–304. https://doi.org/10.1038/s41558-018-0105-1

Oltmanns, M., Straneo, F., Moore, G. W., & Mernild, S. H. (2014). Strong downslope wind events in Ammassalik, southeast Greenland. *Journal of Climate*, *27*(3), 977–993. https://doi.org/10.1175/JCLI-D-13-00067.1

Outten, S. D., Renfrew, I. A., & Petersen, G. N. (2009). An easterly tip jet off Cape Farewell, Greenland. II: Simulations and dynamics. *Quarterly Journal of the Royal Meteorological Society*, *135*, 1934–1949. https://doi.org/10.1002/qj.531

Pennelly, C., Hu, X., & Myers, P. G. (2019). Cross-isobath freshwater exchange within the North Atlantic subpolar Gyre. *Journal of Geophysical Research: Oceans*, *124*, 6831–6853. https://doi.org/10.1029/2019JC015144

Petit, T., Lozier, M. S., Josey, S. A., & Cunningham, S. A. (2020). A new paradigm for Atlantic Ocean deep water formation. *Geophysical Research Letters*, *47*. https://doi.org/10.1029/2020GL091028

Pickart, R., Spall, M., Ribergaard, M., Moore, G. W. K., & Milliff, R. F. (2003). Deep convection in the Irminger Sea forced by the Greenland tip jet. *Nature*, *424*, 152–156. https://doi.org/10.1038/nature01729

Piron, A., Thierry, V., Mercier, H., & Caniaux, G. (2016). Argo float observations of basin-scale deep convection in the Irminger sea during winter 2011–2012. *Deep-Sea Research Part I: Oceanographic Research Papers*, *109*, 76–90. https://doi.org/10.1016/j.dsr.2015.12.012

Piron, A., Thierry, V., Mercier, H., & Caniaux, G. (2017). Gyre-scale deep convection in the subpolar North Atlantic Ocean during winter 2014–2015. *Geophysical Research Letters*, *44*, 1439–1447. https://doi.org/10.1002/2016GL071895

Renfrew, I. A., Outten, S. D., & Moore, G. W. K. (2009). An easterly tip jet off Cape Farewell, Greenland. I: Aircraft observations. *Quarterly Journal of the Royal Meteorological Society*, *135*, 1919–1933. https://doi.org/10.1002/qj.513

Sampe, T., & Xie, S. P. (2007). Mapping high sea winds from space: A global climatology. *Bulletin of the American Meteorological Society*, *88*, 1965–1978. https://doi.org/10.1175/BAMS-88-12-1965

Schulze Chretien, L. M., & Frajka-Williams, E. (2018). Wind-driven transport of fresh shelf water into the upper 30m of the Labrador Sea. *Ocean Science*, *14*(5), 1247–1264. https://doi.org/10.5194/os-14-1247-2018

Shepherd, A., Ivins, E., Rignot, E., Smith, B., van den Brooke, M., Velicogna, I., et al. (2020). Mass balance of the Greenland Ice Sheet from 1992 to 2018. *Nature*, *579*(7798), 233–222. https://doi.org/10.1038/s41586-018-0179-y

Tonboe, R. T., Eastwood, S., Lavergne, T., Sørensen, A. M., Rathmann, N., Dybkjær, G., et al. (2016). The EUMETSAT sea ice concentration climate data record. *The Cryosphere*, *10*(5), 2275–2290. https://doi.org/10.5194/tc-10-2275-2016

Toudal Pedersen, L., Dybkjær, G., Eastwood, S., Heygster, G., Ivanova, N., Kern, S., et al. (2017). *October 5 ESA Sea Ice Climate Change Initiative (Sea_Ice_cci): Sea ice concentration climate data record from the AMSR-E and AMSR-2 instruments at 25km grid spacing* (Version 2.0). Centre for Environmental Data Analysis.

Våge, K., Pickart, R. S., Moore, G. W. K., & Ribergaard, M. H. (2008). Winter mixed layer development in the central Irminger Sea: The effect of strong, intermittent wind events. *Journal of Physical Oceanography*, *38*, 541–565. https://doi.org/10.1175/2007JPO3678.1

Våge, K., Pickart, R. S., Sarafanov, A., Knutsen, Ø., Mercier, H., Lherminier, P., et al. (2011). The Irminger Gyre: Circulation, convection, and interannual variability. *Deep-Sea Research Part I: Oceanographic Research Papers*, *58*, 590–614. https://doi.org/10.1016/j.dsr.2011.03.001

Våge, K., Spengler, T., Davies, H. C., & Pickart, R. S. (2009). Multi-event analysis of the westerly Greenland tip jet based upon 45 winters in ERA-40. *Quarterly Journal of the Royal Meteorological Society*, *135*, 1999–2011. https://doi.org/10.1002/qj.488

Van Aken, H. M., de Jong, M. F., & Yashayaev, I. (2011). Decadal and multi-decadal variability of Labrador Sea Water in the northern North Atlantic Ocean derived from tracer distributions: Heat budget, ventilation, and advection. *Deep-Sea Research, Part I*, *58*, 505–523. https://doi.org/10.1016/j.dsr.2011.02.008

Weijer, W., Coauthors, W., Drijfhout, S. S., Fedorov, A. V., Hu, A., Jackson, L. C., et al. (2019). Stability of the Atlantic Meridional Overturning Circulation: A review and synthesis. *Journal of Geophysical Research: Oceans*, *124*, 5336–5375. https://doi.org/10.1029/2019JC015083

Yang, Q., Dixon, T., Myers, P., Bonin, J., Chambers, D., van den Broeke, M. R., et al. (2016). Recent increases in Arctic freshwater flux affects Labrador Sea convection and Atlantic overturning circulation. *Nature Communications*, *7*, 10525. https://doi.org/10.1038/ncomms10525